Flash microwave sintering of zirconia by multiple susceptors cascade strategy

Guillaume Riquet, Thomas Grippi, Christelle Harnois, Sylvain Marinel, Charles Manière

Flash microwave sintering of zirconia by multiple susceptors cascade strategy

Guillaume Riquet[1*], Thomas Grippi[1], Christelle Harnois[1], Sylvain Marinel[1], Charles Manière[1*]

1. Normandie Univ, ENSICAEN, UNICAEN, CNRS, CRISMAT, 14000, Caen, France

Keywords

Flash sintering; Zirconia; Simulation; Microwave Sintering; Sintering Mechanism

Abstract

In the field of flash sintering, microwave energy represents an interesting way to densify ceramics complex shapes, thanks to a contactless volumetric heating. Attaining a fast and homogeneous heating is a critical parameter and hybrid heating, using silicon carbide susceptors, is generally used. In this study, an original multiple susceptors cascade strategy is developed, using both SiC and 3D-printed ZrO_2 susceptors. This novel configuration follows perfectly the flash heating scheme, even for high heating rates up to 1000 $K.min^{-1}$ and leads to a high stability of the "flash" hybrid heating. Flash microwave sintering produced dense (97% relative density) microstructures within 45 s. Based on comprehensive multiphysics simulations of the overall process, *in-situ* dilatometry measurements, kinetics method analysis and microstructural characterizations, this work highlights the sintering behavior of zirconia and the temperature distribution during flash microwave sintering.

Graphical Abstract

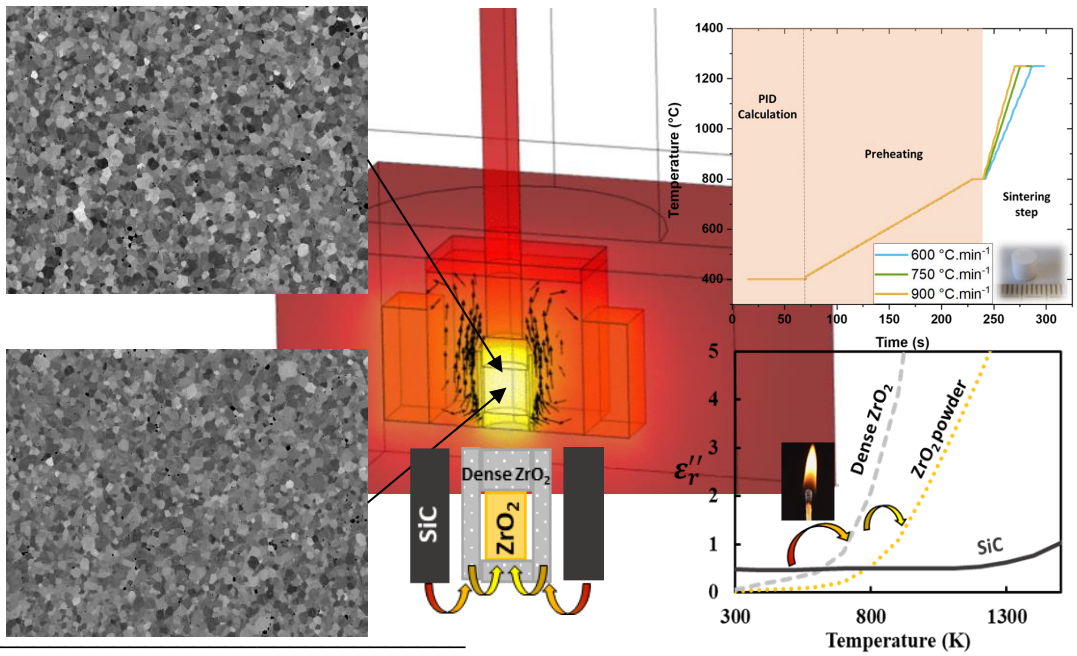

* Corresponding author: Laboratoire de cristallographie et sciences des matériaux (CRISMAT), 6 Bvd du maréchal Juin 14050 CAEN CEDEX 4, France
Ph.: +33.2.31.45.13.69 ; *E-mail address*: guillaume.riquet@ensicaen.fr charles.manière@ensicaen.fr

Nomenclature

C_p Heat capacity ($J \cdot kg^{-1} \cdot K^{-1}$)
T Temperature (K)
κ Thermal conductivity ($W \cdot m^{-1} \cdot K^{-1}$)
Q_e Heat source ($W \cdot m^{-3}$)
φ_{rsa} Surface to ambient radiative heat flux ($W \cdot m^{-2}$)
σ_s Stefan Boltzmann constant (5.67E-8 $W \cdot m^{-2} K^{-4}$)
ϵ Emissivity
T_{air} Air temperature (K)
φ_{csa} Convective heat flux ($W \cdot m^{-2}$)
h_{ia} Surface conductivity ($W \cdot m^{-2} \cdot K^{-1}$)
J Surface radiosity ($W \cdot m^{-2}$)
G Irradiation flux ($W \cdot m^{-2}$)
n Refractive index
$e_b(T)$ Surface radiation produced ($W \cdot m^{-2}$)
ρ_r Reflectivity
φ_{rss} Net inward radiative heat flux ($W \cdot m^{-2}$)
μ_r Complex relative permeability
ε_r Complex relative permittivity
μ_r'' Relative permeability imaginary part
ε_r'' Relative permittivity imaginary part
k_0 Vacuum wave number ($rad \cdot m^{-1}$)
σ Electric conductivity ($S \cdot m^{-1}$)
ε_0 Vacuum permittivity ($8.854187817... \times 10^{-12}$ $F \cdot m^{-1}$)
μ_0 Vacuum permeability ($1.2566370614... \times 10^{-6}$ $T \cdot m \cdot A^{-1}$)
j Imaginary unit
ω Angular frequency ($rad \cdot Hz$)
t Time (s)
$\boldsymbol{E}$ Electric field ($V \cdot m^{-1}$)
$\boldsymbol{H}$ Magnetic field ($A \cdot m^{-1}$)
P_{PID} PID regulated Cavity length (m)
$e(t)$ Regulated - measured temperature error (K)
K_p PID proportional coefficient
K_I PID integral coefficient
K_DPID derivative coefficient
S_{11} Reflective scattering parameter

1. Introduction

Flash sintering is an ultra-rapid sintering process involving complete densification in few seconds. This phenomenon was first discovered at the Colorado University with the work of Cologna *et al.* [1] with the study of the field assisted sintering. The typical configuration of flash sintering involves the application of an electrical field by platinum electrodes on a "dog bone" shape specimen. Under certain imposed field and temperature conditions [2–8], the negative temperature coefficient (NTC) of the resistivity of ceramics, as zirconia, involves an abrupt Joule heating profile. To avoid the melting of the sample, this thermal runaway heating behavior is controlled by a current threshold, at which a transition from voltage control to current control is operated. This conventional flash sintering technique has been adapted to a wide range of ceramics from semi-conductors to dielectrics (ZrO_2 [1,9–11], ZnO [12,13], $BaTiO_3$ [14], $SrTiO_3$ [15], TiO_2 [16], Y_2O_3 [17], Al_2O_3 [18,19]). For metal like materials and for refractory or ultra-refractory ceramics, the flash sintering was adapted to the spark plasma sintering technique (called flash SPS). This approach is interesting as it allows the application of a high pressure (>100 MPa) and imposes an abrupt current profile for conductive materials that have a PTC behavior (positive temperature coefficient of resistivity). Moreover, flash SPS is interesting because it employs graphite foil to preheat the specimen. The activation of its conductivity allows a hybrid heat of the specimen during the sintering, which decreases the thermal gradients generated by the cooling fluxes at the edges [7]. By flash SPS, in sinter-forging configuration, large specimens of refractory ceramics have been produced such as ZrB_2 [20], HfB_2 [21], TiB_2 [22], SiC [23,24], B_4C [25], Co_2MnO_4 [26]. Using an insulated die, it is possible to control the specimen shape and benefits a hybrid heating behavior to impose ultra-rapid densification of various electrical behavior materials like Ni [27], ZrO_2 [28,29] and also $MoSi_2$ [30], SiC [31] or $CaCu_3Ti_4O_{12}$ [32].

Nevertheless, the industrialization of flash sintering is still a far prospect; this requires addressing the inherent challenge of complex shapes and the heterogeneous current density

distributions. Admittedly, ceramics can be produced by continuous flash sintering and the demonstration of the production of tile shapes has been made by Lucideon Ltd in the UK [33]. Using flat electrodes, it was possible to produce 2D complex shapes of zirconia, coupling robocasting with flash sintering [34]. In a recent article in *Science*, Wang *et al.* obtained flat shapes and lattice structures of different ceramics (Al_2O_3, YSZ, oxide-based garnet-type solid state electrolytes) by reactive flash sintering, starting from 3D printed structures [35]. By coupling flash SPS with the deformed interface method [36], a recent study showed the possibility to obtain 30 mm gears in zirconia by flash SPS, with a submicronic microstructure [37]. All these advances are very promising but for 3D complex shapes, a contactless volumetric heating would represent a better solution for the flash sintering of oxides.

Thus, microwave energy appears as a very interesting candidate to impose a flash sintering behavior to a working space where complex shapes can be ultra-rapidly sintered. Microwave can easily couple with semiconductors and dielectrics by dipolar interaction. Under constant microwave electromagnetic field, NTC materials, as zirconia, reproduce the characteristic flash sintering heating response under voltage control [38]. Microwave flash sintering has been studied at the gyrotron frequency 24 GHz [39–41] and magnetron frequency 2.45 GHz [42,43]. Microwave energy has also shown a certain potential for the flash sintering of metal powders under certain conditions [44–46]. In the microwave domain, hybrid heating is a central aspect to balance the volumetric heat of the specimen, the edge of the material where cooling fluxes generate thermal gradients and, for NTC materials, the destructive hot spot phenomena [38,47–51]. To succeed in this hybrid heating, susceptors in microwave coupling materials like SiC, are generally employed. These materials help to stabilize the temperature field and initiate the heating of dielectrics that couple only at high temperatures. One of the main differences with conventional flash sintering is the way the microwave flash sintering is controlled. As stated before, the voltage/current control switch is employed in conventional flash sintering to limit the destructive behavior of the thermal runaway. For flash microwave

sintering, this control system cannot be applied and a PID controlled power generator has to regulate the apparent temperature of the specimen under an ultra-rapid heating cycle.

The aim of this paper is to investigate an efficient way to impose the ultra-rapid heating and sintering of zirconia specimens. To control the heating phenomena, a PID control system is used and a multiple susceptors cascade configuration is specifically designed to homogenize the temperature field. By this method, the initial heating is induced by SiC susceptors and the flash hybrid heating of the sample is ensured by a dense 3D printed zirconia susceptors. In this paper, microwave flash sintering of zirconia is studied, with multiphysics simulation of the overall process, detailed *in-situ* dilatometry studies and microstructural characterizations.

2. Experiment and method

2.1. Microwave heating physics simulation

To highlight the electromagnetic-thermal behavior of the microwave assembly used during this study, a simulation study was conducted with the software COMSOL Multiphysics. First, the electromagnetic behavior was solved at room temperature to plot the internal distribution of the $\vec{E}$ and $\vec{H}$ fields and define the cavity resonant length. To do so, Maxwell's equations were combined and expressed in COMSOL as [17,48] :

$$\nabla \times (\mu_r^{-1} \nabla \times \boldsymbol{E_r}) = k_0^2 \left(\varepsilon_r - \frac{j\sigma}{\omega\, \varepsilon_0}\right) \boldsymbol{E_r} \quad (1)$$

with $\boldsymbol{E_r}$ the harmonic electric field expression $\boldsymbol{E} = \boldsymbol{E_r} exp(j\omega t)$.

Then, the fully coupled electromagnetic-thermal model was developed and calculated the heat transfer (2) with the volumetric dissipated power (3). The temperature dependence of electromagnetic properties is considered for each used material. This can be found in the appendix.

$$\rho C_p \frac{\partial T}{\partial t} + \nabla.(-\kappa \nabla T) = Q_e \quad (2)$$

$$Q_e = \frac{\omega}{2}(\varepsilon_0 \varepsilon_r'' \boldsymbol{E}^2 + \mu_0 \mu_r'' \boldsymbol{H}^2) \quad (3)$$

For the electromagnetic boundary conditions, all internal metallic surfaces are assumed perfectly reflective and a TE_{10} port is inserted at the generator location to simulate both the generator and the isolator. The simulation also includes a numerical PID on the forward microwave power which imposes the thermal cycle to the specimen as in the experiment. The PID has the following expression:

$$P_{PID} = K_p e(t) + K_I \int_0^t e(t)d\tau + K_D \frac{de(t)}{dt} \quad (4)$$

For the thermal boundary conditions, all the heat transfers were modeled. Air convection was defined through the Navier-Stokes fluid dynamic equations as described in a previous work [52]. For the insulation box and the overall assembly, two surface cooling fluxes conditions were outlined, with respectively, convective (5) and radiative (6) heat transfers:

$$\varphi_{csa} = h_{ia}(T_{air} - T) \quad (5)$$

$$\varphi_{rsa} = \sigma_s \epsilon ({T_{air}}^4 - T^4) \quad (6)$$

The surface radiosity J ($W.m^{-2}$) and the net inward radiative heat flux φ_{rss} ($W.m^{-2}$) were expressed by :

$$J = \rho_r G + \epsilon e_b(T) = \rho_r G + \epsilon n^2 \sigma_s T^4 \quad (7)$$

$$\varphi_{rss} = \epsilon(G - e_b(T)) \quad (8)$$

2.2. Method and experimental configuration

To perform "contactless flash sintering", a 2.45 GHz single mode microwave configuration from SAIREM was used. As shown in figure 1a, the cavity was tuned to TE_{105}, promoting interactions of the materials with the electrical $\vec{E}$ field. To create favorable conditions for the "flash microwave sintering", a specific insulation box and a multiple susceptors cascade strategy were employed. Previous works [53] have demonstrated that cooling fluxes compensation is one of the key parameters to succeed in ultra-rapid microwave sintering. Thus, a specific design of the assembly has been created, as described in figure1b. First, ZrO_2

susceptors were 3D printed by fused filament fabrication (Zetamix ZrO_2 filament Z-WH1CER from Nanoe). Different shapes (small cylinders [7.5 mm in diameter, 2 mm high] and thin hollow cylinder [8 mm in inner diameter, 1 mm in thickness, 12 mm high]) were printed. Those dimensions are designed to be flush with the sample after debinding and sintering. Organic compounds were removed in acetone at 50 °C during 4 hours and then debinded in air in an oven at 500 °C with a slow heating rate (8 °C.min^{-1}). The different zirconia susceptors were finally sintered at 1475 °C during 1 hour. Thus, in this assembly, the zirconia green sample can be surrounded by dense 3D-printed ZrO_2 susceptors and centered inside aluminosilicate insulation box. Two 20x20 mm² silicon carbide susceptors are also employed to initiate the heat in hybrid conditions in the overall assembly. To optimize the heating, the SiC susceptors are placed in the electrical field vector plane. The microwave dissipation is therefore optimal and the configuration is less sensitive to the offsets of the maximum electric field location [45–47].

To fully understand the principle of this multiple susceptors cascade strategy, it is important to pay attention to the dielectric properties of the materials, as shown in figure 1c. Based on that, it is quite easy to understand that SiC susceptors heat preferentially at low temperatures and contribute to initiate the heating of the dense 3D-printed ZrO_2 susceptors. As the relative permittivity ε_r" of this material rapidly increases with temperature, the heating of this second set of susceptors becomes more and more efficient. Therefore, ZrO_2 susceptors heating is able to follow the flash heating scheme, even for high heating rates up to 1000 K/min, and leads to high stability hybrid heating of the green material.

The temperature was measured on ZrO_2 cylindrical susceptors by infrared pyrometer through an aperture machined in the thermal insulation box. The emissivity was fixed at 0.7. It is important to keep in mind that every temperature that will be presented in the next sections are processes temperatures and not the sample temperature. An autoadaptative PID system was also used to ensure a good regulation quality of the imposed sintering cycles. In addition, a displacement sensor with alumina rod (magnescale DS812SLR from Sensel Measurements, measure length 12 mm, resolution 1 µm) was used to to follow the specimen shrinkage during

the sintering. For all experiments, two *in situ* displacement measurements were performed. The first one was conducted to record the sintering shrinkage of the sample and a second one was done on a fully sintered specimen to subtract the tooling thermal expansion. So that, the shrinkage curves presented attest of the material sintering behavior only.

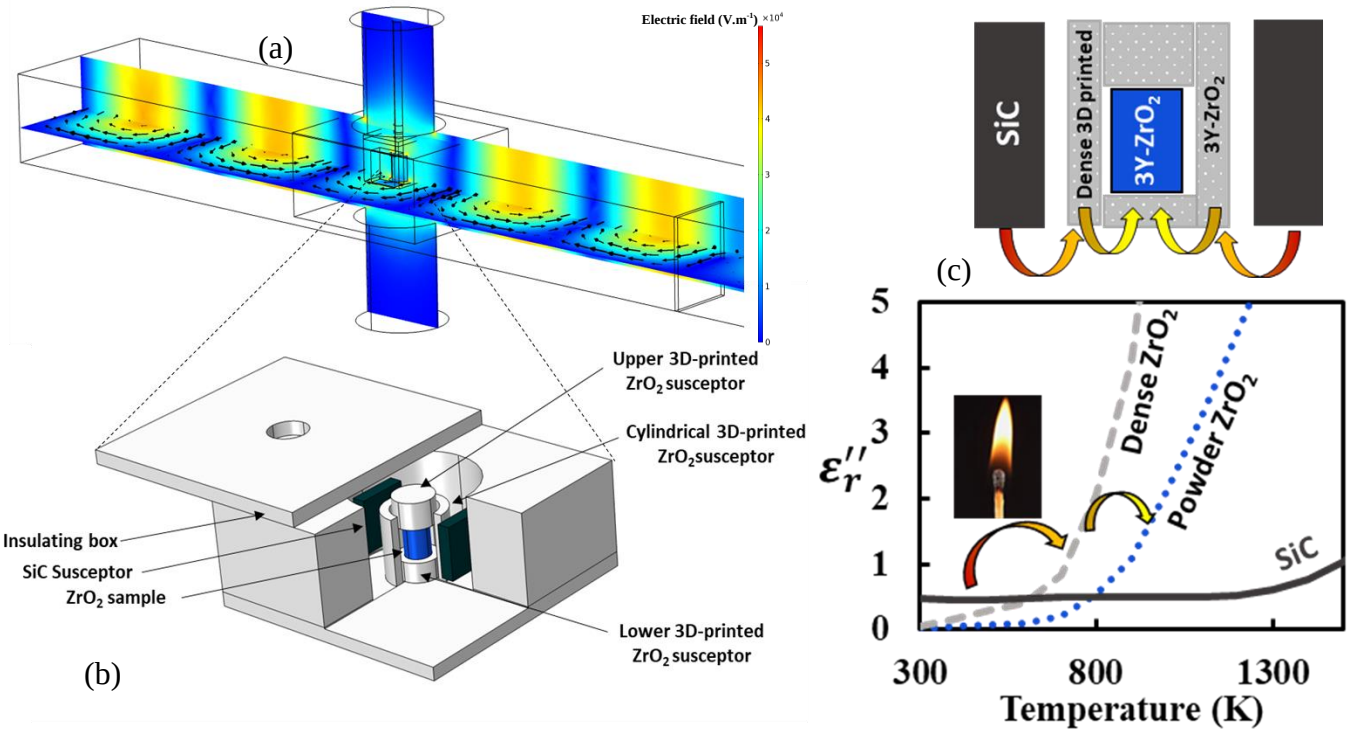

Figure 1: Flash microwave sintering configuration, (a) electric field at resonance, (b) assembly of the insulation box (c) Evolution of the relative permittivity imaginary part ε_r" for the different materials of the heated zone

2.3. Materials shaping, sintering and characterizations

In this study, ZrO_2 powder from Tosoh (3mol% Y_2O_3 "3YZS-BE", 40 nm) was used as raw material. Pellets (6 mm in diameter, 6 mm in thickness) were shaped by uniaxial pressure followed by cold isostatic pressing at 400 MPa. The green samples were close to 55% of the theoretical density (ρ=6.1 g.cm^{-3}). The imposed sintering cycles are reported in figure 2. First, the autoadaptive PID system was initialized and the PID coefficients were calculated. Then, the preheating of the green sample and the overall assembly started up to 800°C during few seconds. The *in-situ* displacement measurements confirmed that this process temperature is low

enough to avoid sintering of the green sample. The sintering step started thereafter with the rapid increase of temperature up to 1250°C with three heating rates of precisely 600, 750 and 900°C.min^{-1} followed by a 20s dwell at high temperature. The obtained dilatometry data were used in a Wang & Raj study *via* a homemade octave-forge script. The density of the flash sintered materials was measured by Archimedes method in ethanol. Each sample was cut in half and polished down to 1 µm with a diamond suspension, and 0.25 µm with colloidal silica. The microstructural characterizations were carried out using a scanning electron microscope (SEM JEOL JSM 7200F). The average grain size was estimated by linear intercept method over 200 grains of different micrographs to ensure a good reliability.

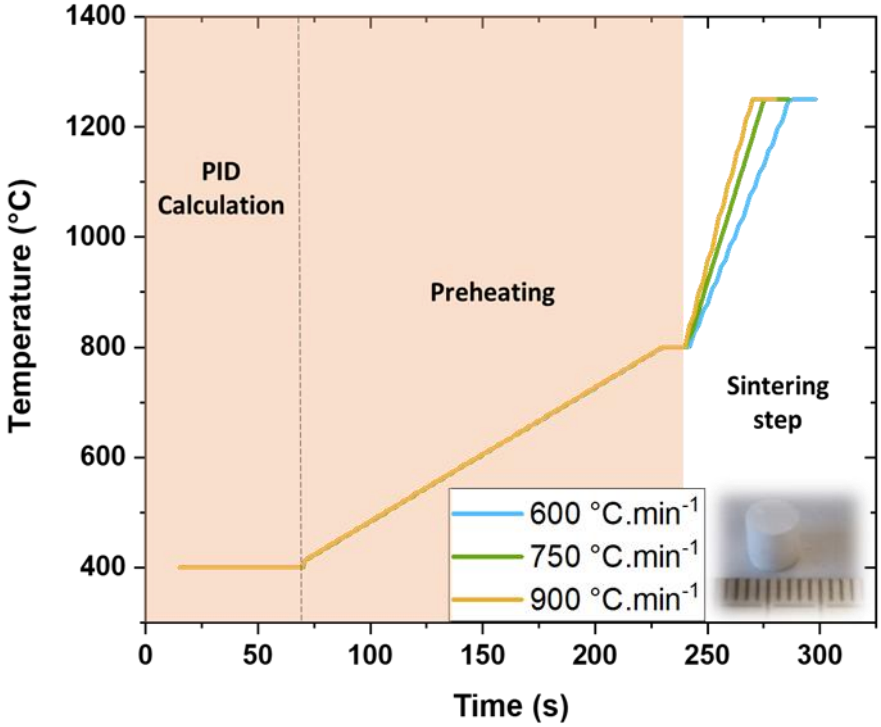

Figure 2: Set heating cycles used for "flash" microwave sintering.

3. Results and discussions

3.1. Microwave sintering explorations by increasing heating ramp

The recorded data in terms of microwave power, thermal cycle and relative shrinkage are presented in figure 3 for the experiments at 600, 750 and 900 °C.min^{-1}. Despite these high heating rates, the regulation system follows perfectly the set temperature cycle, allowing a good repeatability of the different experiments. Although microwaves were stopped at the end of the

final dwell, a cooling rate had to be set to collect the final thermal and microwave data. The dissipated power was between 100 and 300 W, with a slight increase of the power at the beginning of the sintering step to follow the rapid heating rate. The maximum forward power used was 900W. The cavity and impedance tuner were adjusted to ensure higher heating efficiency during the sintering step. The chosen sintering parameters (process temperature, heating rates, and dwell time) appeared relevant based on the *in situ* displacement measurements. Indeed, figure 3 showed that sintering took place only during the high increase of temperature from 800 °C to 1250 °C, and appeared complete in less than 60 s for all experiments, which is consistent with term "flash microwave sintering". It is important to remind that these temperatures are processing temperatures and in any case not the real temperatures the green samples were subjected to.

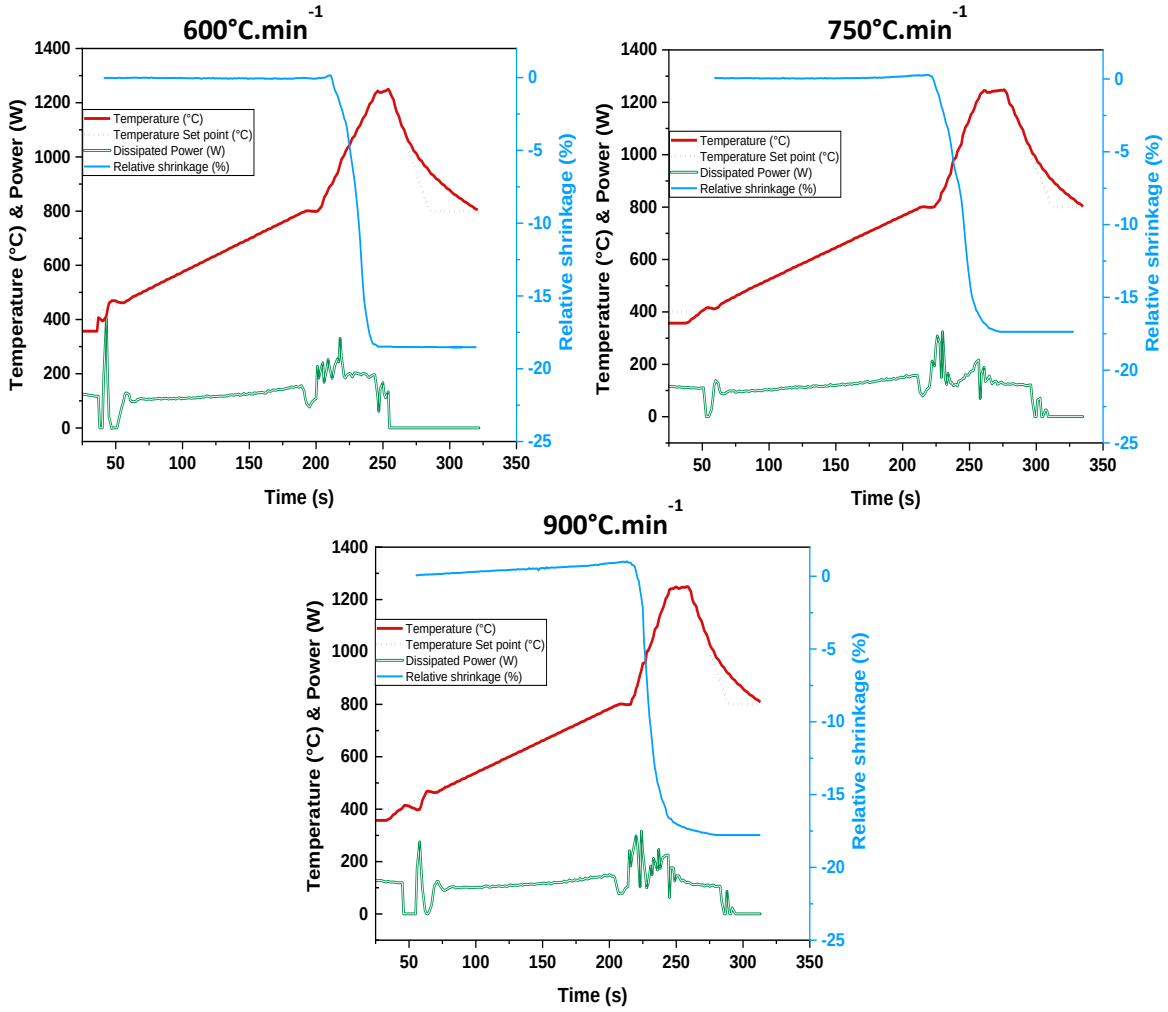

Figure 3: Recorded microwave/thermal/shrinkage data for the experiments at 600, 750, and 900 °C/min.

The sintering seemed successful and complete for all heating rates with a final relative shrinkage from 17.5% to 18%. A previous work showed that cracks might appear for high heating rates above 400 °C.min^{-1} due to important thermal gradients [53]. In our case, the design of the hybrid assembly had been rethought to reduce cooling effects and achieve optimal conditions for flash microwave sintering. As a result, all samples have integrity, only a few micro-crack remains at microstructure level. The density of each sample was measured by Archimedes method and confirmed the obtaining of dense material up to 96% of relative density.

3.2. Estimation of material temperature based on electromagnetic-thermal-fluid-dynamic simulation

To highlight the specificities of flash microwave sintering, a fully coupled electromagnetic-thermal-fluid-dynamic simulation was carried out. Electromagnetic waves and heat transfers (by air convection, conduction and surface-to-surface radiation) were considered to compute the electromagnetic and temperature fields. As an example, the simulated temperature fields of the 600 °C/min heating rate are reported in figure 4. As expected, using the multiple susceptors cascade strategy, the simulation clearly shows that SiC susceptors preferentially heat during early stages of the flash microwave sintering (figure 4a). Then, the heating element switches from SiC to ZrO_2 susceptors and becomes more and more efficient as the temperature increases (figure 4b).

To estimate the material temperature and its evolution during flash microwave sintering, temperature probes were virtually introduced at different locations. This simulation highlights several key points to improve our understanding of this flash microwave sintering. Figure 5 shows clearly that the material temperature is hotter than the process temperature. As expected, this first result is consistent with microwave heating, known to be volumetric and external zone are cooled by convection/radiation.

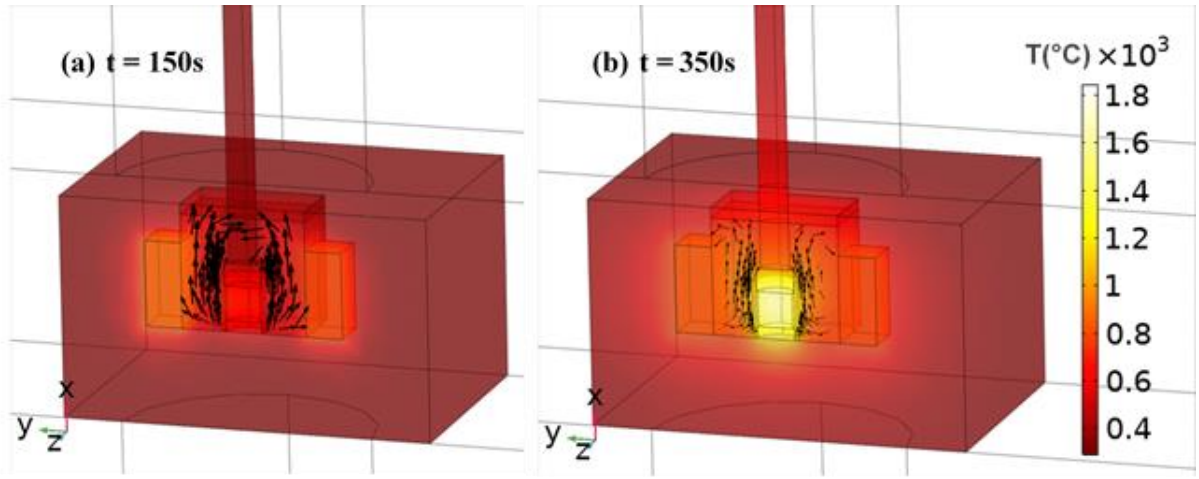

Figure 4: Simulated thermal field at (a) t = 150s and (b) t = 250s of the 600C.min^{-1}test

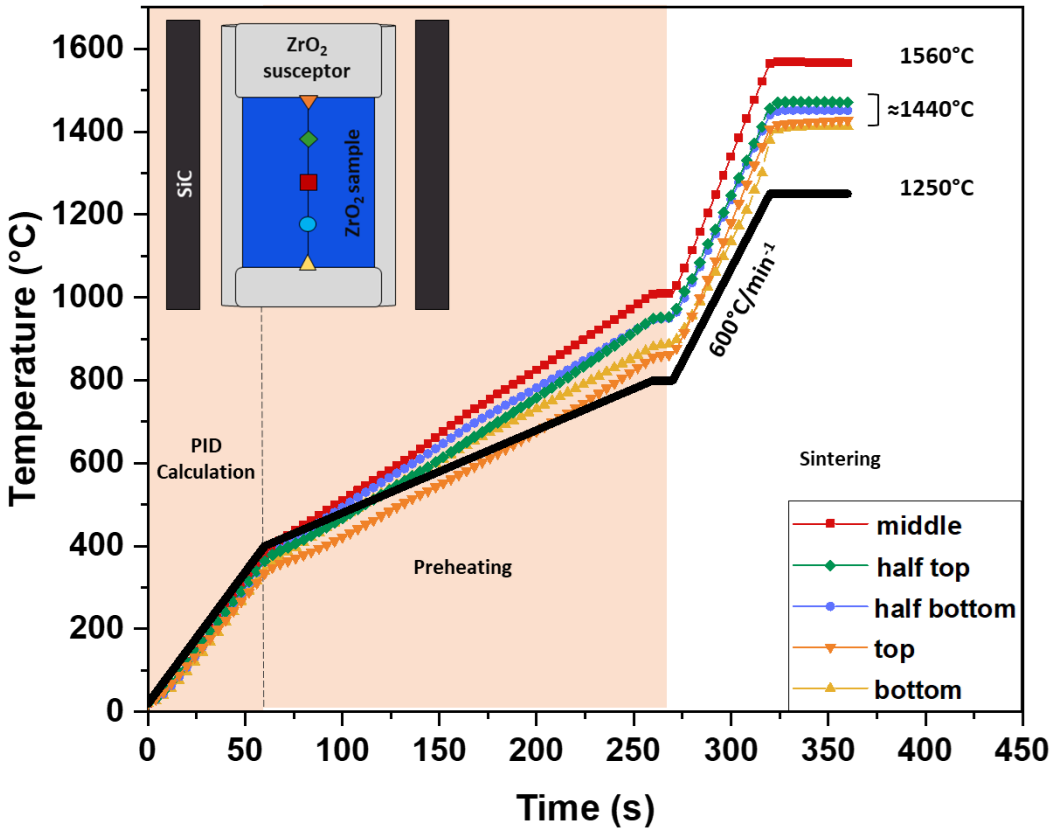

Figure 5: Simulated temperature evolution during flash microwave heating with heating rate of 600°C.min^{-1}.

During the preheating, non-compliance of the set heating rate is observed. The system tends towards higher temperatures than the ones measured on the susceptor, which will be very useful to impose, subsequently, the very high heating rates. The intermediate dwell, used to regulate the runaway, takes place at higher temperatures (up to 1000 °C) than the initial set parameter (800 °C). That information, although important, does not represent any problem as any shrinkage or displacement of the green sample has been measured during this preheating step. For the final sintering step, the high heating rate of 600 °C.min^{-1} is preserved thanks to the thermal runaway. The simulated temperatures indicate that the entire material appears to be stabilizing around 1440 °C during the final dwell (simulated local temperature ranging from 1410 °C to 1470 °C). It is also worthy to mention that hot spot may appear in the center of the sample. However, the presence of the 3D printed zirconia suceptor considerably limit the thermal gradients with temperature differences less then 120K. As presented in figure 5, the middle of the sample could reach high temperatures up to 1560 °C, which could considerably affect the sintering and the final microstructures.

The same simulations have been undertaken for the other heating rates: 750 °C.min^{-1} and 900 °C.min^{-1}. The key information are presented in table 1. As the simulated material temperature is much higher than the process temperature, it is important to consider it and to adjust the temperature in the operation and interpretation of the experimental data. Although the sintering step is completed in a very short amount of time, less than 60 seconds, the presence of the very high temperatures reached in the center of the material may have an important impact on the microstructures and has to be explored.

This simulation shows the heating using the susceptors cascade strategy limits the thermal gradients to a controllable temperature distribution. In appendix A, we have explored the rapid sintering of 3D printed zirconia gears. This shows lager sizes quickly imply heterogeneity and multimode or lower monomode frequency is required for complex shapes or higher scales.

Table 1 : Resume of the key simulated temperatures for the three different heating rates.

Heating rates	Process T°	Simulated temperature during final dwell	
		Mean T°	Highest T°
600 °C.min^{-1}	1250°C	1440 °C	1560 °C
750 °C.min^{-1}	1250°C	1436 °C	1552 °C
900 °C.min^{-1}	1250°C	1430 °C	1540 °C

3.3. Microstructures and sintering behavior

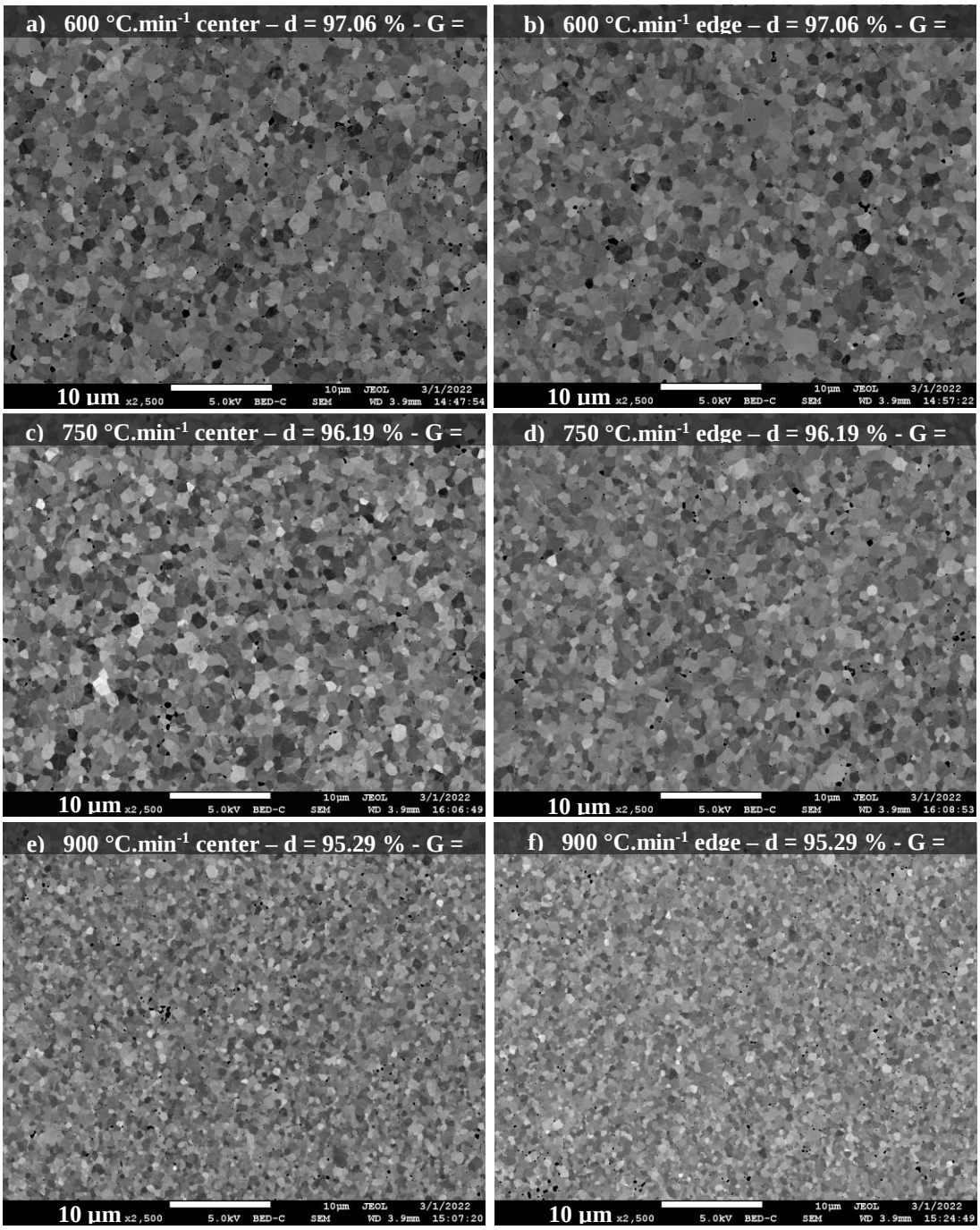

Figure 6: SEM images of the tests at 600°C.min^{-1} (a, b), 750°C.min^{-1} (c, d),

All the microstructures obtained after the flash microwave sintering are shown in figure 6. As observed, all the materials are fully densified and present relative density ranging from 95.3% (figure 6e, 6f) to 97% (figure 6a, 6b), respectively for the highest heating rate at 900 °Cmin^{-1} and for the one at 600 °C.min^{-1}. Concurrently, grain size distribution is centered on 1.6 µm for the heating rate at 600 °C.min^{-1} and remains low, around 750 nm, for the highest heating rate, as shown in figure 6e, 6f. Comparing the microstructures between the center and the edge, no significant heterogeneity is observed in terms of grain size or pores distribution which remain in intergranular region. Although the simulation showed previously that the temperature is higher in the center of the sample, the microstructures are similar regardless of the location or the heating rates. This suggests that the temperature distribution field within the material is relatively homogenous. Therefore, it is possible to argue that the duration of the sintering step is too short to allow a significant impact of the central high temperature on the microstructure.

Based on that assumption, the process temperature has been adjusted to take into account the simulated mean temperature, which appears to be consistent and more in line with microstructural observations. As a result, the corrected relative density curves of the different experiments are presented in figure 7. The multiple susceptors cascade strategy and the high heating rates allow to significantly minimize the duration of the sintering, ranging from 30 to 45 seconds, suitable with the naming of flash microwave sintering. The sintering temperatures range is 1000 – 1500 °C and remains consistent with our previous work realized on the same ZrO_2 powder at lower heating rates [53]. To go further with this flash microwave dilatometry data, a Wang & Raj (WR) kinetics method was conducted. This technique is well known for determining the activation energy of sintering. The general expression for the instantaneous sintering rate $\dot{\rho}$ is expressed by [54]:

$$\dot{\rho} = A\frac{e^{-Q/RT}}{T}\ \frac{f(\rho)}{d^n} \tag{9}$$

with d the grain size, f(ρ) is a function of the specimen relative density, Q the activation energy, A represents a material parameter, R the gaz constant and T is the absolute temperature.

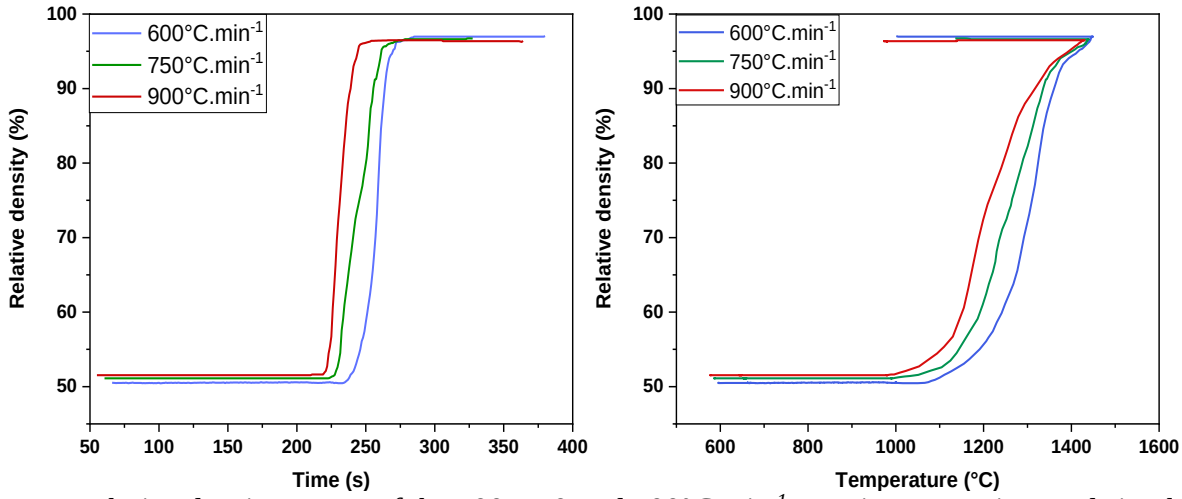

Figure 7: Relative density curves of the 600, 750 and 900°C.min^{-1}experiments vs time and simulated specimen temperatures.

Based on dilatometry measurements, the density can be expressed as a function of time, therefore it is possible to obtain Arrhenius plots at fixed values of density. Considering the 65%-85% range of density, and assuming that the grain size remains nearly constant on this range of density [54,55], the previous expression becomes:

$$ln\left(T\dot{T}\frac{d\rho}{dT}\right) = -\frac{Q}{RT} + \ln[f(\rho)] + \ln \mathrm{A} - \mathrm{n} \ln \mathrm{d} \qquad (10)$$

Figure 8 presents the regression plots of sintering rate logarithms *vs* 1/RT at different fixed relative densities giving the sintering activation energy by the slope of the curves. With WR kinetics method, the sintering activation energy was estimated to be close to 128 kJ.mol^{-1}. Although certain precautions must be taken in estimating the temperature, the obtained value is significantly different from the classic thermal activation energy of conventional sintered 3YSZ ceramics. The densification activation energy for flash microwave sintering is therefore much lower than the ones reported for conventional sintering by Wang *et al.* (615 ± 80 kJ.mol^{-1}) [56], Matsui *et al.* (647 ± 48 kJ.mol^{-1}) [57] and even for microwave sintering by Maniere *et al.* (225 kJ.mol^{-1}) at 400 °C.min^{-1} [53]. This sintering activation energy tends to approach the value reported for flash sintering by Ren *et al.* (85 ± 7 kJ.mol^{-1}) [58]. The controlled flash microwave sintering process of zirconia undoubtedly differed from conventional densification, suggesting a special sintering regime due to the high heating rates. Different phenomena have already been put forward to explain this behavior. Among them, the formation of abundant oxygen vacancies combined with Joule heating appeared to be very important to incubate and initiate flash

sintering [53, 58, 59]. The interaction of the microwave field with the effective electric charges of vacancies also enhances the ponderomotive forces and accelerates the shrinkage rate during microwave sintering [53,60].

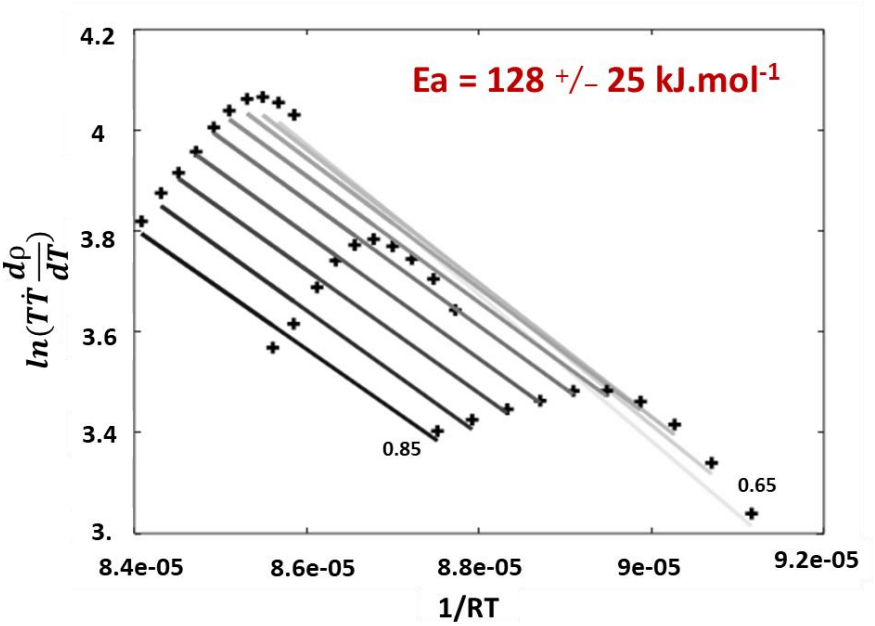

Figure 8: Sintering activation energy Wang and Raj plots for zirconia in flash microwave sintering.

4. Conclusion

In this study, the flash microwave sintering of 3YSZ samples was investigated, at the lab scale, using an original multiple susceptors cascade strategy. The multiphysics simulation revealed a high stability hybrid heating, despite the presence of higher temperatures in the core of the material due to the volumetric microwave heating. Nonetheless, as sintering took place in a very short amount of time, the temperature difference within the sample was found to have no significant impact on the final microstructures, in this case. Zirconia ceramics were flash sintered in less than 45 s with dense (up to 97% of relative density), homogeneous microstructures and fine grains. The densification kinetics of flash microwave sintered 3YSZ were also investigated. With an apparent activation energy of 128 ± 25 kJ.mol^{-1}, this flash microwave process tends to approach the low flash sintering activation energy reported in the literature. Therefore, this flash microwave sintering process, using multiple susceptors cascade strategy, represents an interesting alternative adapted for ceramics, even with a very low

electrical conductivity like alumina or complex shapes, where conventional flash sintering remains limited.

Appendix

Appendix A, explorative rapid microwave sintering tests on 3D printed zirconia gears.

This article shows 6mm thick zirconia specimens can be produced without excessive thermal gradients. Explorative tests have been done (in figure A) on 3D printed gear shapes and still using the same susceptor cascade strategy. The same cycle of the article has been used à 100°C/min and 600°C/min up to 1250°C with 10s holding. The first test at 100°C/min shows a sample with a relatively homogeneous sintering of the shape without crack. When rapid heating rate is used (600°C/min), the sintering is less homogeneous and a crack appears in the porous zone. This type of defect looks like to be due to a heterogeneous field as 2.45GHz impose a very limited working field zone. To pursue the study on shapes close to centimetric scales, multimode or 915MHz monomode configurations should be preferred. However, these test shows the rapid sintering of complex shape is not a long-term prospect.

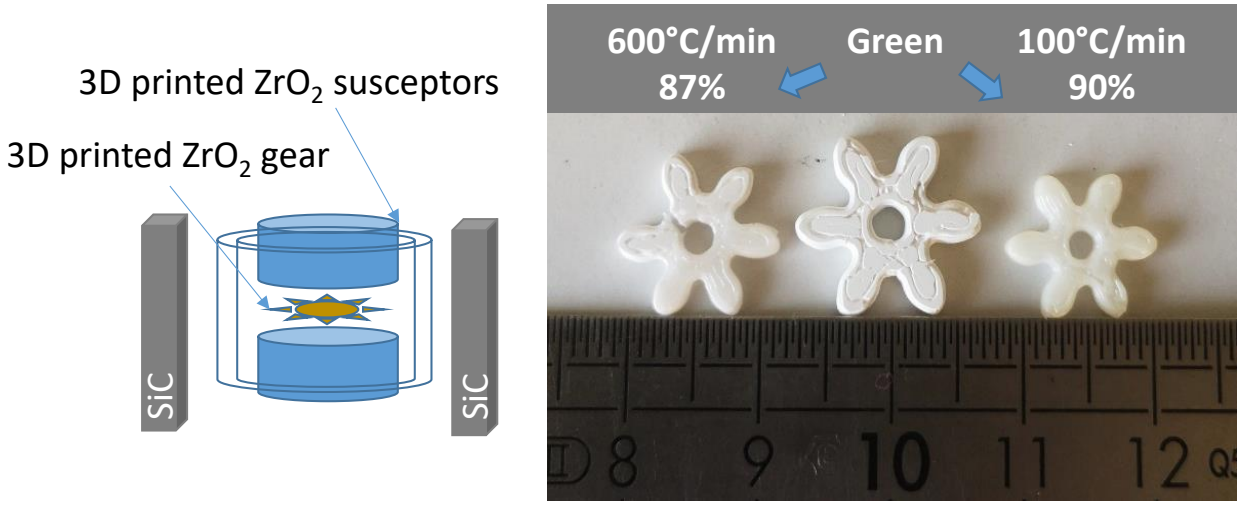

Figure A, Explorative rapid microwave sintering tests on 3D printed zirconia gear specimens.

Appendix B, materials properties in the simulations.

The physical properties used for the simulation are reported in the table B.

Table B Temperature dependent electromagnetic-thermal properties of zirconia, SiC susceptor and insulator with: T the absolute temperature, D the relative density.

	Temperature range (K)	Zirconia [15,24]	Temperature range (K)	Silicon carbide susceptor [24,31]	Temperature range (K)	Insulator [16]
Cp	273-1473 1473-2200	(43+2.35 T-0.34E-3 T^2+4.25E-6 T^3-2.09E-9 T^4+4.06E-13 T^5) 638	273-673 673-1573 1573-2200	-8.35+3.08T-0.00293 T^2+1.0268E-6 T^3 772+0.431 T-2.10E-5 T^2 1400	273-2200	-5.31E-4.T^2+1.25.T+5.18E2
κ	273-2200	(1.96-2.32E-4 T+6.33E-7 T^2-1.91E-10 T^3) × (1-1.5 × (1-D))	273-2200	192-0.326 T+2.74E-4 T^2-7.71E-8 T^3	273-2200	1.40E-4.T+1.70E-2
ρ	273-2200	(6132 -9.23E-2 T-7.26E-5 T^2+4.58E-8 T^3-1.31E-11 T^4) × D	273-2200	2977+0.0510 T-2.29E-4 T^2+2.98E-7 T^3-1.92E-10 T^4+4.77E-14 T^5	273-2200	-1.04E-02.T+4.43E2
ϵ [27]	273-2200	0.7	273-2200	0.9	273-2200	0.83
ε_r'	273-2200	-5.38-4.34E-3 T+2.22E1 D+1.37E-2 T D	273-2200	1.88E-06 T^2-1.67E-03 T+6.4	273-2200	5.03E-8.T^2+1.37E-5.T+1.5
ε_r''	273-673 673-873 873-1073 1073-2200	1.48E-1-5.76E-4 T-4.55E-01 D+1.77E-03 T D 3.82-6.03E-3 T-1.172E1 D+1.85E-2 T D 1.56E1-1.95E-2 T-4.74E1 D+5.94E-2 T D 3.25E1-3.86E-2 T-7.64E1 D+8.46E-2 T D+3.82E-6 T^2+1.07 D^2	273-2200	2.36E-12 T^4-7.15E-09 T^3+7.72E-06 T^2-3.43E-03 T+9.92E-01	273-2200	2.50E-09.T^2-1.64E-6.T+3.96E-4
μ_r'	273-2200	1	273-2200	1	273-2200	1
μ_r''	273-2200	0	273-2200	0	273-2200	0

Acknowledgements

This study was funded by the French National Research Agency (ANR), project ULTRARAPIDE N°ANR-19-CE08-0033-01.

The help and support of Christelle Bilot and Jérôme Lecourt are gratefully acknowledged.

Data availability

The raw/processed data required to reproduce these findings cannot be shared at this time due to technical or time limitations.

Credit authorship contribution statement

Guillaume Riquet: Conceptualization, Experimentation, Characterizations, Modeling, Writing, Review & editing; **Christelle Harnois** Review & editing; **Thomas Grippi** Homemade script development, Calculation; Review & editing **Sylvain Marinel:** Review & editing, **Charles Manière:** Conceptualization, Supervision, Modeling, Review & editing;

References

[1] M. Cologna, B. Rashkova, R. Raj, Flash Sintering of Nanograin Zirconia in <5 s at 850°C, J. Am. Ceram. Soc. 93 (2010) 3556–3559. doi:10.1111/j.1551-2916.2010.04089.x.

[2] R. Raj, M. Cologna, A.L.G. Prette, V. Sglavo, Methods of flash sintering, Patent US 20130085055 A1, US 20130085055 A1, 2013. https://www.google.com/patents/US20130085055.

[3] M. Yu, S. Grasso, R. Mckinnon, T. Saunders, M.J. Reece, Review of flash sintering: materials, mechanisms and modelling, Adv. Appl. Ceram. 116 (2017) 24–60. doi:10.1080/17436753.2016.1251051.

[4] R.I. Todd, Flash Sintering of Ceramics: A Short Review, in: Proc. IV Adv. Ceram. Appl. Conf., Atlantis Press, Paris, 2017: pp. 1–12. doi:10.2991/978-94-6239-213-7_1.

[5] M. Biesuz, V.M. Sglavo, Flash sintering of ceramics, J. Eur. Ceram. Soc. 39 (2019) 115–143. doi:10.1016/j.jeurceramsoc.2018.08.048.

[6] J. Luo, The scientific questions and technological opportunities of flash sintering: From a case study of ZnO to other ceramics, Scr. Mater. 146 (2018) 260–266. doi:10.1016/j.scriptamat.2017.12.006.

[7] G.M. Jones, M. Biesuz, W. Ji, S.F. John, C. Grimley, C. Manière, C.E.J. Dancer, Promoting microstructural homogeneity during flash sintering of ceramics through thermal management, MRS Bull. 46 (2021) 59–66. doi:10.1557/s43577-020-00010-2.

[8] C.E.J. Dancer, Flash sintering of ceramic materials, Mater. Res. Express. 3 (2016)

102001. doi:10.1088/2053-1591/3/10/102001.
[9] R.I. Todd, E. Zapata-Solvas, R.S. Bonilla, T. Sneddon, P.R. Wilshaw, Electrical characteristics of flash sintering: thermal runaway of Joule heating, J. Eur. Ceram. Soc. 35 (2015) 1865–1877. doi:10.1016/j.jeurceramsoc.2014.12.022.
[10] M. Biesuz, L. Pinter, T. Saunders, M. Reece, J. Binner, V. Sglavo, S. Grasso, Investigation of Electrochemical, Optical and Thermal Effects during Flash Sintering of 8YSZ, Materials (Basel). 11 (2018) 1214. doi:10.3390/ma11071214.
[11] M.C. Steil, D. Marinha, Y. Aman, J.R.C. Gomes, M. Kleitz, From conventional ac flash-sintering of YSZ to hyper-flash and double flash, J. Eur. Ceram. Soc. 33 (2013) 2093–2101. doi:10.1016/j.jeurceramsoc.2013.03.019.
[12] C. Schmerbauch, J. Gonzalez-Julian, R. Röder, C. Ronning, O. Guillon, Flash Sintering of Nanocrystalline Zinc Oxide and its Influence on Microstructure and Defect Formation, J. Am. Ceram. Soc. 97 (2014) 1728–1735. doi:10.1111/jace.12972.
[13] J. Nie, Y. Zhang, J.M. Chan, S. Jiang, R. Huang, J. Luo, Two-step flash sintering of ZnO: Fast densification with suppressed grain growth, Scr. Mater. 141 (2017) 6–9. doi:10.1016/j.scriptamat.2017.07.015.
[14] J.-C. M'Peko, J.S.C. Francis, R. Raj, Field-assisted sintering of undoped BaTiO3: Microstructure evolution and dielectric permittivity, J. Eur. Ceram. Soc. 34 (2014) 3655–3660. doi:10.1016/j.jeurceramsoc.2014.04.041.
[15] A. Karakuscu, M. Cologna, D. Yarotski, J. Won, J.S.C. Francis, R. Raj, B.P. Uberuaga, Defect Structure of Flash-Sintered Strontium Titanate, J. Am. Ceram. Soc. 95 (2012) 2531–2536. doi:10.1111/j.1551-2916.2012.05240.x.
[16] S.K. Jha, J.M. Lebrun, K.C. Seymour, W.M. Kriven, R. Raj, Electric field induced texture in titania during experiments related to flash sintering, J. Eur. Ceram. Soc. 36 (2016) 257–261. doi:10.1016/j.jeurceramsoc.2015.09.002.
[17] H. Yoshida, K. Morita, B.-N. Kim, Y. Sakka, T. Yamamoto, Reduction in sintering temperature for flash-sintering of yttria by nickel cation-doping, Acta Mater. 106 (2016) 344–352. doi:10.1016/j.actamat.2016.01.037.
[18] M. Cologna, J.S.C. Francis, R. Raj, Field assisted and flash sintering of alumina and its relationship to conductivity and MgO-doping, J. Eur. Ceram. Soc. 31 (2011) 2827–2837. doi:10.1016/j.jeurceramsoc.2011.07.004.
[19] M. Biesuz, V.M. Sglavo, Flash sintering of alumina: Effect of different operating conditions on densification, J. Eur. Ceram. Soc. 36 (2016) 2535–2542. doi:10.1016/j.jeurceramsoc.2016.03.021.
[20] S. Grasso, T. Saunders, H. Porwal, O. Cedillos-Barraza, D.D. Jayaseelan, W.E. Lee, M.J. Reece, Flash Spark Plasma Sintering (FSPS) of Pure ZrB 2, J. Am. Ceram. Soc. 97 (2014) 2405–2408. doi:10.1111/jace.13109.
[21] J. Zou, S. Grasso, L.-F. Liu, H.-B. Ma, M. Reece, J. Binner, Flash spark plasma sintering of HfB2 ceramics without pre-sintering, Scr. Mater. 156 (2018) 115–119. doi:10.1016/j.scriptamat.2018.07.026.
[22] R. McKinnon, S. Grasso, A. Tudball, M.J. Reece, Flash spark plasma sintering of cold-Pressed TiB 2 - h BN, J. Eur. Ceram. Soc. 37 (2017) 2787–2794. doi:10.1016/j.jeurceramsoc.2017.01.029.
[23] S. Grasso, T. Saunders, H. Porwal, B. Milsom, A. Tudball, M. Reece, Flash Spark Plasma Sintering (FSPS) of α and β SiC, J. Am. Ceram. Soc. 99 (2016) 1534–1543. doi:10.1111/jace.14158.
[24] E.A. Olevsky, S. Rolfing, Y.S. Lin, A. Maximenko, Flash spark-plasma sintering of SiC powder, in: 10th Pacific Rim Conf. Ceram. Glas. Technol. Coronado, CA, Coronado, 2013: p. 32.
[25] B. Niu, F. Zhang, J. Zhang, W. Ji, W. Wang, Z. Fu, Ultra-fast densification of boron carbide by flash spark plasma sintering, Scr. Mater. 116 (2016) 127–130. doi:10.1016/j.scriptamat.2016.02.012.
[26] A.L.G. Prette, M. Cologna, V. Sglavo, R. Raj, Flash-sintering of Co2MnO4 spinel for

solid oxide fuel cell applications, J. Power Sources. 196 (2011) 2061–2065. doi:10.1016/j.jpowsour.2010.10.036.
[27] C. Manière, G. Lee, E.A. Olevsky, All-Materials-Inclusive Flash Spark Plasma Sintering, Sci. Rep. 7 (2017) 15071. doi:10.1038/s41598-017-15365-x.
[28] C. Manière, C. Harnois, G. Riquet, J. Lecourt, C. Bilot, S. Marinel, Flash spark plasma sintering of zirconia nanoparticles: Electro-thermal-mechanical-microstructural simulation and scalability solutions, J. Eur. Ceram. Soc. (2021). doi:10.1016/j.jeurceramsoc.2021.09.021.
[29] T. Hérisson de Beauvoir, Z. Ghomari, G. Chevallier, A. Flaureau, A. Weibel, C. Elissalde, F. Mauvy, R. Chaim, C. Estournès, Flash Spark Plasma Sintering of 3YSZ: Modified sintering pathway and impact on grain boundary formation, J. Eur. Ceram. Soc. 41 (2021) 7762–7770. doi:10.1016/j.jeurceramsoc.2021.08.013.
[30] E. Zapata-Solvas, D. Gómez-García, A. Domínguez-Rodríguez, R.I. Todd, Ultra-fast and energy-efficient sintering of ceramics by electric current concentration, Sci. Rep. 5 (2015) 8513. doi:10.1038/srep08513.
[31] C. Manière, G. Lee, J. McKittrick, A. Maximenko, E.A. Olevsky, Graphite creep negation during flash spark plasma sintering under temperatures close to 2000 °C, Carbon N. Y. 162 (2020) 106–113. doi:10.1016/j.carbon.2020.02.027.
[32] C. Manière, G. Riquet, S. Marinel, Dielectric properties of flash spark plasma sintered BaTiO3 and CaCu3Ti4O12, Scr. Mater. 173 (2019) 41–45. doi:10.1016/j.scriptamat.2019.07.048.
[33] E. Sortino, J. Lebrun, A. Sansone, R. Raj, Continuous flash sintering, J. Am. Ceram. Soc. 101 (2018) 1432–1440. doi:10.1111/jace.15314.
[34] B. Yang, J. Cho, X.L. Phuah, H. Wang, X. Zhang, Flash sintering of additively manufactured 3YSZ gears, J. Am. Ceram. Soc. 104 (2021) 3828–3832. doi:10.1111/jace.17835.
[35] C. Wang, W. Ping, Q. Bai, H. Cui, R. Hensleigh, R. Wang, A.H. Brozena, Z. Xu, J. Dai, Y. Pei, C. Zheng, G. Pastel, J. Gao, X. Wang, H. Wang, J.-C. Zhao, B. Yang, X. (Rayne) Zheng, J. Luo, Y. Mo, B. Dunn, L. Hu, A general method to synthesize and sinter bulk ceramics in seconds, Science (80-.). 368 (2020) 521–526. doi:10.1126/science.aaz7681.
[36] C. Manière, E. Nigito, L. Durand, A. Weibel, Y. Beynet, C. Estournès, Spark plasma sintering and complex shapes: The deformed interfaces approach, Powder Technol. 320 (2017) 340–345. doi:10.1016/j.powtec.2017.07.048.
[37] C. Manière, G. Lee, E.A. Olevsky, Flash sintering of complex shapes, Appl. Mater. Today. 26 (2022) 101293. doi:10.1016/j.apmt.2021.101293.
[38] C. Manière, T. Zahrah, E.A. Olevsky, Inherent heating instability of direct microwave sintering process: Sample analysis for porous 3Y-ZrO2, Scr. Mater. 128 (2017) 49–52. doi:10.1016/j.scriptamat.2016.10.008.
[39] Y. Bykov, S. Egorov, A. Eremeev, V. Kholoptsev, I. Plotnikov, K. Rybakov, A. Sorokin, On the Mechanism of Microwave Flash Sintering of Ceramics, Materials (Basel). 9 (2016) 684. doi:10.3390/ma9080684.
[40] Y. V. Bykov, S. V. Egorov, A.G. Eremeev, V. V. Kholoptsev, K.I. Rybakov, A.A. Sorokin, Flash Microwave Sintering of Transparent Yb:(LaY) 2 O 3 Ceramics, J. Am. Ceram. Soc. 98 (2015) 3518–3524. doi:10.1111/jace.13809.
[41] Y. V. Bykov, S. V. Egorov, A.G. Eremeev, I. V. Plotnikov, K.I. Rybakov, A.A. Sorokin, V. V. Kholoptsev, Flash Sintering of Oxide Ceramics under Microwave Heating, Tech. Phys. 63 (2018) 391–397. doi:10.1134/S1063784218030052.
[42] C. Manière, G. Lee, E. Torresani, J.F. Gerling, V. V. Yakovlev, D. Martin, E.A. Olevsky, Flash microwave pressing of zirconia, J. Am. Ceram. Soc. 103 (2020) 4110–4121. doi:10.1111/jace.17072.
[43] S. Marinel, E. Savary, M. Gomina, Sintering of CuO and ZnO in a Single Mode Microwave Cavity with Shrinkage Control, J. Microw. Power Electromagn. Energy. 44 (2010) 57–63. doi:10.1080/08327823.2010.11689770.

[44] J. Perelaer, M. Klokkenburg, C.E. Hendriks, U.S. Schubert, Microwave Flash Sintering of Inkjet-Printed Silver Tracks on Polymer Substrates, Adv. Mater. 21 (2009) 4830–4834. doi:10.1002/adma.200901081.
[45] J. Perelaer, R. Jani, M. Grouchko, A. Kamyshny, S. Magdassi, U.S. Schubert, Plasma and Microwave Flash Sintering of a Tailored Silver Nanoparticle Ink, Yielding 60% Bulk Conductivity on Cost-Effective Polymer Foils, Adv. Mater. 24 (2012) 3993–3998. doi:10.1002/adma.201200899.
[46] C. Manière, G. Lee, T. Zahrah, E.A. Olevsky, Microwave flash sintering of metal powders: From experimental evidence to multiphysics simulation, Acta Mater. 147 (2018) 24–34. doi:10.1016/j.actamat.2018.01.017.
[47] M. Oghbaei, O. Mirzaee, Microwave versus conventional sintering: A review of fundamentals, advantages and applications, J. Alloys Compd. 494 (2010) 175–189. doi:10.1016/j.jallcom.2010.01.068.
[48] K.I. Rybakov, E.A. Olevsky, E. V. Krikun, Microwave Sintering: Fundamentals and Modeling, J. Am. Ceram. Soc. 96 (2013) 1003–1020. doi:10.1111/jace.12278.
[49] V. V Yakovlev, S.M. Allan, M.L. Fall, H.S. Shulman, Computational Study of Microwave Processing of thermal runaway in microwave processing Zirconia, in: J.C.E. Tao (Ed.), Microw. RF Power Appl., Toulouse, 2011: pp. 303–306. https://users.wpi.edu/~vadim/AMPERE-2011-125.pdf.
[50] C. Manière, T. Zahrah, E.A. Olevsky, Fully coupled electromagnetic-thermal-mechanical comparative simulation of direct vs hybrid microwave sintering of 3Y-ZrO2, J. Am. Ceram. Soc. 100 (2017) 2439–2450. doi:10.1111/jace.14762.
[51] S. Marinel, F. Valdivieso, C. Manière, Frittage de céramiques par chauffage micro-ondes, Tech. l'ingénieur, Verres Céramiques. (2021). doi:10.51257/a-v1-n4808.
[52] C. Manière, F. Borie, S. Marinel, Impact of convection and radiation on direct/hybrid heating stability of field assisted sintering, J. Manuf. Process. (2020) https://doi.org/10.1016/j.jmapro.2020.04.075
[53] C. Manière, C. Harnois, G. Riquet, T. Grippi, S. Behar-Lafenetre, S. Marinel, Rapid microwave sintering of centimetric zirconia: scalability and electromagnetic-thermal-fluid-dynamic simulation, J. Am. Ceram. Soc. (2022)
[54] G. Bernard-Granger, C. Guizard, Spark plasma sintering of a commercially available granulated zirconia powder: I. Sintering path and hypotheses about the mechanism(s) controlling densification, Acta Mater. 55 (2007) 3493-3504 https://doi.org/10.1016/j.actamat.2007.01.048
[55] C. Manière, G. Lee, J. McKittrick, S. Chan, E.A. Olevsky, Modeling zirconia sintering trajectory for obtaining translucent submicronic ceramics for dental implant applications, Acta Mater. 188 (2020) 101-107 https://doi.org/10.1016/j.actamat.2020.01.061
[56] J. Wang and R. Raj, Activation Energy for the Sintering of Two-Phase Alumina/Zirconia Ceramics, J. Am. Ceram. Soc., 74 (1991) 1959-1963, DOI: 10.1111/j.1551-2916.2006.01415.x
[57] K. Matsui, N. Ohmichi, M. Ohgai, N. Enomoto, J. Hojo, Sintering Kinetics at Constant Rates of Heating: Effect of Al_2O_3 on the Initial Sintering Stage of Fine Zirconia Powder, J. Am. Ceram. Soc., 88 (2005) 3346-3352, DOI: 10.1111/j.1551-2916.2005.00620.x
[58] K. Ren, Q. Wang, Y. Lian, Y. Wang, Densification kinetics of flash sintered 3mol% Y_2O_3 stabilized zirconia, J. Alloys. Comp. 747 (2018) 1073-1077 https://doi.org/10.1016/j.jallcom.2018.02.308
[59] Y. Gao, F. Liu, D. Liu, J. Liu, Y. Wang, L. An, Electrical-field induced nonlinear conductive behavior in dense zirconia ceramic. Journal of Materials Science & Technology, 33(8) (2017), 897–900 doi:10.1016/j.jmst.2017.03.005
[60] E.A. Olevsky, A. L. Maximenko, E.G. Grigoryev, Ponderomtive effects during contact formation in microwave sintering, Modelling Sumul. Mater. Sci. Eng. 21 (2013) 055022 DOI: 10.1088/0965-0393/21/5/055022